ACS APPLIED MATERIALS & INTERFACES

Research Article

www.acsami.org

Reversible Lithium Storage in Manganese 1,3,5-Benzenetricarboxylate Metal–Organic Framework with High Capacity and Rate Performance

Sandipan Maiti,[†,‡] Atin Pramanik,[†,‡] Unnikrishnan Manju,[†,§] and Sourindra Mahanty*[,†,‡]

[†]CSIR-Central Glass & Ceramic Research Institute, Kolkata 700032, India

[‡]CSIR-Network Institutes for Solar Energy (NISE), New Delhi, India

Supporting Information

ABSTRACT: Metal organic frameworks (MOFs) with diverse structural chemistry are being projected as futuristic electrode materials for Li-ion batteries. In this work, we report synthesis of Mn-1,3,5-benzenetricarboxylate MOF by a simple solvothermal method and its application as an anode material for the first time. Scanning electron microscopy of the synthesized MOF shows a bar shaped morphology where these bars, about 1 μm wide and of varied lengths between 2 and 20 μm, are made of porous sheets containing mesoporous walls and macroporous channels. The MOF anode, when examined in the potential window of 0.01−2.0 V versus Li/Li$^+$, shows high specific capacities of 694 and 400 mAh g^{-1} at current densities of 0.1 and 1.0 A g^{-1} along with good cyclability, retention of capacity, and sustenance of the MOF network. Ex situ X-ray diffraction, Fourier transform infrared, and X-ray photoelectron spectroscopy studies on the electrode material at different states of charge suggest that the usual conversion reaction for Li storage might not be applicable in this case. Conjugated carboxylates being weakly electron withdrawing ligands with a stronger $\pi-\pi$ interaction, a probable alternative Li storage mechanism has been proposed that involves the organic moiety. The present results show promise for applying Mn-1,3,5-benzenetricarboxylate MOF as high performance <2 V anode.

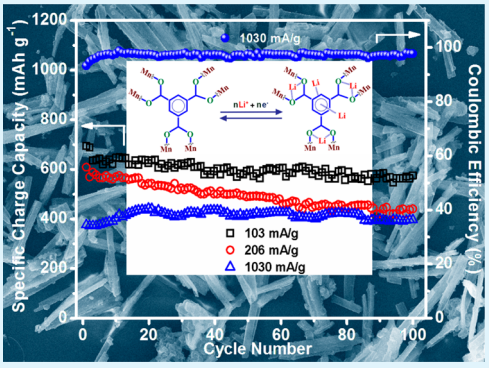

KEYWORDS: *metal organic framework, solvothermal reaction, lithium-ion battery, energy storage*

1. INTRODUCTION

Along with significant advancements toward technological maturity of conventional lithium-ion battery (LIB) based on the reversible exchange of Li$^+$ ions between a graphite anode and the mixed metal-oxide cathode, it has been realized that developing a new electrode materials alternative to carbonaceous anodes is the key to meet the ever increasing demand for energy density and power density.[1−3] Metal−organic frameworks (MOFs) are crystalline porous coordination polymers composed of 1D, 2D, or 3D networks resulting from the bonding of metal ions with polyfunctional organic molecules. MOFs have found diverse applications in catalysis,[4] chemical separation,[5] gas storage,[6] sensor,[7] and drug delivery[8] due to their high surface area and their ability to react with small molecules in addition to many unique attributes such as controlled pore size, chiral channels, and redox activity. The coordination preference of the central metal ion and the symmetry of the organic linker directly dictate the number of ligands that can bind to the metal and in which orientation, thus providing an opportunity to control the size and shape of the resulting pores. Such kind of 3D architectures with specific structural arrangements with controlled pores often offer improved electrochemical properties, for example, better electrolyte accessibility and higher diffusion rates. Therefore, it is not surprising that MOFs, with their interesting structural chemistry, are being emerged in recent years as promising electrodes in LIBs.[9−13] Tarascon et al.[10,11] have first reported a Fe based MIL-53 MOF [$Fe(OH)_{0.8}F_{0.2}(O_2C-C_6H_4-CO_2)$] as cathode utilizing $Fe^{2+}-Fe^{3+}$ redox properties, albeit with a low capacity (75 mAh g^{-1}). Since then, several MOFs were investigated either as a cathode or as an anode material. Among the anodes (Table S1, Supporting Information), Zn and Ni based MOFs, namely, Zn_4O(1,3,5-benzenetribenzoate)$_2$ and Ni_2(1,4,5,8-naphthalenetetracarboxylate), resulted in the formation of Li_2O and corresponding metal (Zn or Ni, respectively) due to conversion reactions and subsequent breakdown of the MOF network.[9,13] Saravanan et al.[12] have reported Li storage in formate bridged Zn/Co based MOFs [$M_3(HCOO)_6$] also through conversion reaction. Similarly, Liu et al.[14] have studied manganese-based layered coordination polymer [Mn-(tfbdc)(4,4-bpy)$(H_2O)_2$] where the authors demonstrated a conversion reaction from Mn(II) to Mn(0) during the discharge (lithiation) process. More recently, Lin et al.[15] have shown that a functionalized Zn-imidazole MOF can

Received: April 20, 2015
Accepted: July 9, 2015
Published: July 9, 2015

DOI: 10.1021/acsami.5b03414
ACS Appl. Mater. Interfaces 2015, 7, 16357−16363

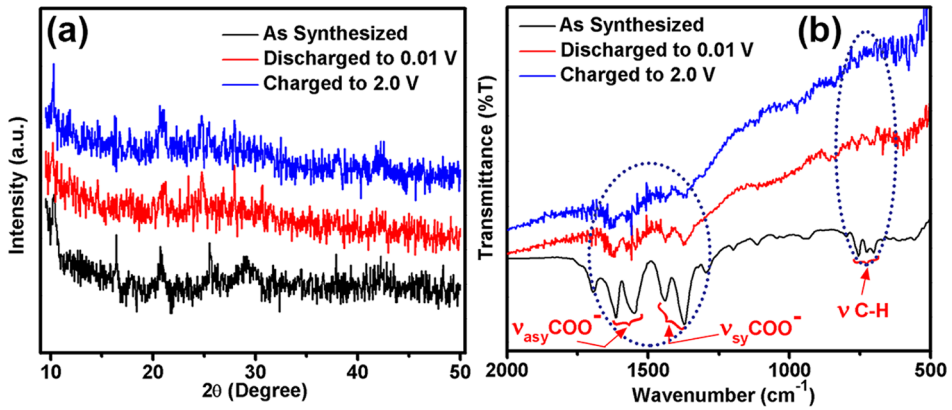

Figure 1. (a) X-ray diffractograms and (b) FTIR spectra of Mn-BTC MOF in the as-synthesized form, at the fully discharged state at 0.01 V, and at the fully charged state at 2.0 V.

store Li inside the pores with specific capacity of 150 mAh g^{-1} at 100 mA g^{-1}. These stimulating studies demonstrate the potential of MOFs as LIB electrode, but until now, a high performance MOF could not be developed, which is stable in organic carbonate electrolytes upon repeated cycling and has the ability to deliver a high capacity with good rate performance, and more importantly, possesses a Li insertion/extraction potential suitable for LIB anode (i.e., < 2.0 V vs Li/Li^+). It transpires from the available literature that redox participation of the transition metal ions has been central to the conversion mechanism of Li storage in MOF where generally the MOF network is destroyed during cycling. On the other hand, intercalation or insertion mechanism often leads to low capacity values. It is probable that the redox processes may also occur in the organic linkers. In such cases, it would be possible to combine the rigidity of the inorganic clusters and flexibility of organic ligands without direct participation of the central metal ion in the redox process, thus sustaining the 3D network of the MOF. Here, selection of organic linker is crucial, as the chemical stability of a MOF in LIB compatible electrolyte, especially within a potential gradient, depends on the metal ligand linkage. Armand et al.[16] have shown that carboxylates being weakly electron withdrawing ligands could act as redox centers for coordination with Li. Similarly, LiO^tBu grafted UiO-66 (1,4-benzenedicarboxylate) based MOF[17,18] and lithium coordination polymers based on carboxylates[19] are found to preserve structural integrity and crystallinity in a LIB-like environment. Inspired by these motivational works, here we have synthesized 1,3,5-benzenetricarboxylate based MOF where manganese is the central atom (henceforth, referred as Mn-BTC MOF) and investigated its reversible lithium insertion–extraction properties as an anode material in Li-ion coin cells. Presence of an aromatic core in the conjugated carboxylates might have stronger $\pi-\pi$ interactions stabilizing the 3D structure of the MOF. We show here that probable involvement of the organic moiety in Li-storage leads to sustenance of the MOF network upon cycling and achievement of the highest specific capacity (694 mAh g^{-1}) reported until now within a voltage window of 0.01–2.0 V along with an excellent rate performance.

2. EXPERIMENTAL SECTION

2.1. Synthesis of Mn-BTC MOF. All chemicals, $Mn(NO_3)_2{\cdot}4H_2O$ (98+%, Acros Organics, USA), C_2H_5OH (Merck, Germany), trimesic acid (1,3,5-H_3BTC) (~95%, Merck, Germany), were used as obtained.

Mn-BTC MOF was synthesized by a simple solvothermal method in a closed glass vessel container. At first, 1.88 g (7.5 mmol) of $Mn(NO_3)_2$ $4H_2O$ was dissolved in 50 mL of C_2H_5OH under constant stirring. Then, a separate solution was prepared by dissolving 0.875 g (4.16 mmol) of trimesic acid (1,3,5-H_3BTC) in 30 mL of C_2H_5OH and was added to the manganese nitrate solution slowly under constant stirring to obtain a clear solution. The resulting solution was transferred to a glass vessel, and the reaction was performed in closed conditions by keeping on a hot plate at 160 °C for 4 days under autogenous pressure. The resulting light brown powder was centrifuged, washed with ethanol, dried at 120 °C for 12 h, and then kept inside a desiccator until further use. The Mn-BTC MOF, thus synthesized, was used for characterization without any further material activation.

2.2. Material Characterization. As-synthesized Mn-BTC MOF powder and Mn-BTC MOF electrodes at different state of charge were analyzed by X-ray diffraction (XRD) in the 2θ range 8°–50° at a scanning rate of 2° min^{-1} by an X-ray diffractometer (Philips X'Pert, The Netherlands) with a Cu–Kα radiation at 40 kV and 40 mA. A BOMEN infrared spectrophotometer was used to record Fourier transform infrared (FTIR) spectra of the as-synthesized Mn-BTC MOF powder and Mn-BTC MOF electrodes at different state of charge in the wavenumber range of 4000–400 cm^{-1} in transmission mode.

The probable composition of the Mn-BTC MOF was estimated from thermogravimetric analysis (TGA), inductively coupled plasma atomic emission spectroscopy (ICP-AES), and elemental analysis. TGA of the Mn-BTC MOF was carried out in air at a heating rate of 10 °C min^{-1} using a Simultaneous Thermal Analyzer (STA449F, Netzsch, Germany). ICP-AES was performed using Spectra Analytical Instrument, Germany by dissolving the Mn-BTC MOF in concentrated HNO_3. Elemental analysis was performed with a Vario-Micro V2.0.11 elemental (CHNSO) analyzer.

Microstructure and morphology of the synthesized Mn-BTC MOF were investigated by a ZEISS Supra 35 (Germany) field emission scanning electron microscope (FESEM) and a Tecnai G^2 30ST (FEI) transmission electron microscope (TEM) operating at 300 kV. Brunauer–Emmett–Teller (BET) surface area measurements were carried out at 77.3 K using a Quantachrome (USA) Autosorb surface analyzer.

To understand the oxidation states of the central atom, X-ray photoelectron spectroscopy (XPS) (model: PHI 5000 VERSA PROBE-II) analysis was performed with the synthesized Mn-BTC MOF powder and also with the Mn-BTC MOF electrode at the fully discharged state (at 0.01 V) in thin pellet form.

2.3. Electrochemical Measurements. Electrochemical properties of the prepared composites were evaluated by fabricating 2032 type coin cells versus Li/Li^+. For fabrication of the working electrodes, Mn-BTC MOF, Super-P carbon, and polyvinylidene fluoride (PVDF) were homogeneously mixed in a weight ratio of 70:20:10 in n-methyl-2-

DOI: 10.1021/acsami.5b03414
ACS Appl. Mater. Interfaces 2015, 7, 16357–16363

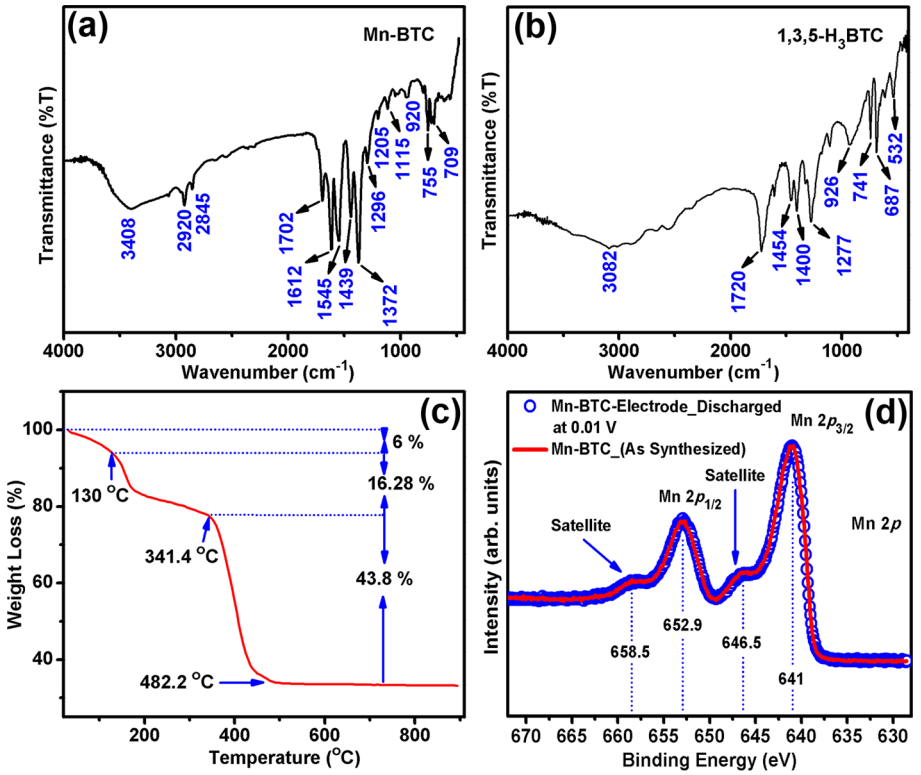

Figure 2. (a, b) FTIR spectra of Mn-BTC MOF and 1,3,5-H_3BTC; (c) TGA profile of Mn-BTC MOF; and (d) high-resolution XPS spectra of Mn-BTC MOF before and after full discharge.

pyrrolidone (NMP) to form a slurry. The slurry was then coated on a 15 μm thick copper foil (current collector) and dried in a vacuum oven at 110 °C for 6 h. After the coated foil was pressed at 4.0 ton inch^{-2}, circular disks of 15 mm in diameter were cut and used as electrode. Typical active mass loading in the electrodes was 1.5−2.0 mg. Coin cells were assembled with these electrodes using Li metal as counter as well as reference electrode, $LiPF_6$ in EC/DMC (1:2 v/v) as electrolyte and Celgard 2300 as separator within an argon filled glovebox (M'BRAUN, Germany), where the moisture and oxygen levels were both kept below 0.5 ppm. Cyclic voltammetry of the cells was carried out by a galvanostat−potentiostat (PGSTAT 30, Autolab,The Netherlands) between 0.01 and 2.0 V at a scanning rate of 0.1 mV s^{-1}. Gavanostatic charge−discharge measurements were carried out using an automatic battery tester (BT2000, Arbin, USA) in the same potential window. Electrochemical impedance spectra were recorded on a galvanostat−potentiostat (PGSTAT302N, Autolab,The Netherlands) in the frequency range of 10 mHz to 1 MHz with an AC amplitude of 10 mV.

3. RESULTS AND DISCUSSION

3.1. Physical Characterization. The carboxylate functional groups of trimesic acid could act as nucleation sites for heterogeneous nucleation of Mn-BTC MOF and subsequent crystal growth.[20] However, the solvent used for synthesis plays a crucial role, and it has been observed that the crystallinity depends on the amount of solvent occluded inside the pores.[20] Thermal removal of solvent leads to significant amorphization of BTC-bridged manganese MOFs due to switching of pore structures. As a result, the powder X-ray diffractogram of the synthesized Mn-BTC MOF (Figure 1a) did not show well-defined diffraction peaks. Therefore, following the approach adopted by Taylor et al.,[21] a combination of results obtained from FTIR, ICP-AES, TGA, and elemental analysis was used to establish its formation and estimation of the probable composition. Further, XPS analysis was performed to ascertain

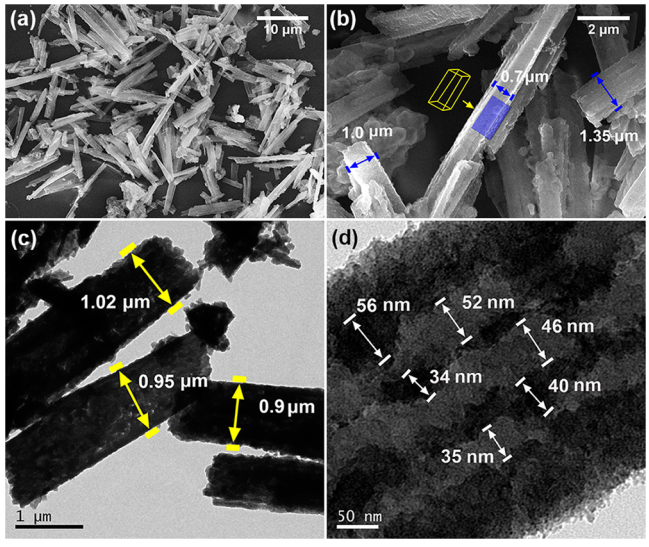

Figure 3. (a, b) FESEM micrographs and (c, d) TEM images of the synthesized Mn-BTC MOF at low and high magnifications.

the electronic states of the central metal atom. Figure 2, panel a represents the FTIR spectrum obtained from Mn-BTC MOF. The corresponding spectrum for 1,3,5-H_3BTC is also shown in Figure 2, panel b for comparison. It is observed that in the FTIR spectrum of Mn-BTC MOF, the characteristic bands (ν_{OH}, 3082 cm^{-1}; $\nu_{C=O}$, 1720 cm^{-1}; $\delta_{C=O}$, 532 cm^{-1}) of the nonionized carboxyl groups of 1,3,5-BTC disappear, and new bands appear in the regions 1612−1545 cm^{-1} (asymmetric stretching vibrations of $-COO^-$), 1433−1372 cm^{-1} (symmetric stretching vibrations of $-COO^-$), and at 755 cm^{-1} (ring-out-of-plane vibration of the 1,3,5-substituted benzene

DOI: 10.1021/acsami.5b03414
ACS Appl. Mater. Interfaces 2015, 7, 16357−16363

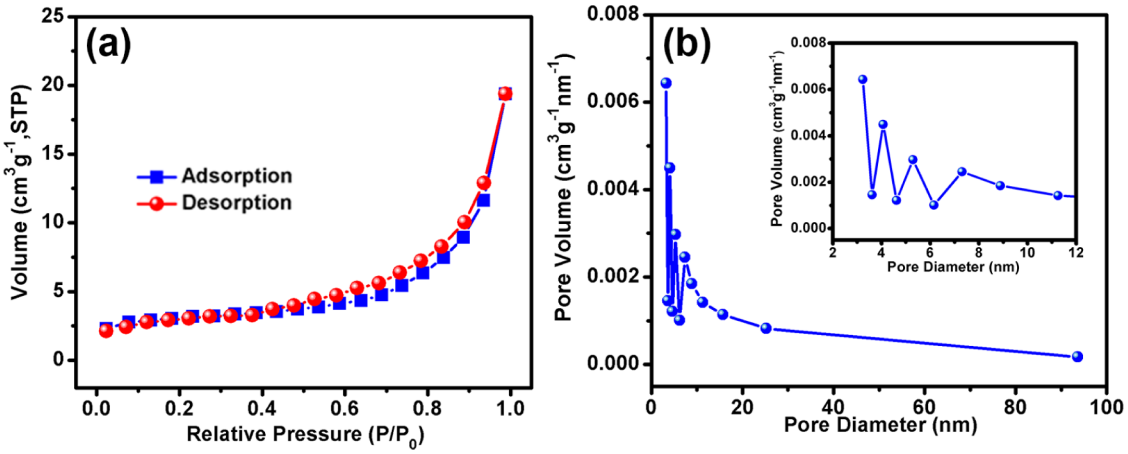

Figure 4. (a) N_2 adsorption−desorption isotherm and (b) pore size distributions of the synthesized Mn-BTC MOF.

core of the linker molecules). These new bands prove that the manganese ions have been coordinated with the 1,3,5-BTC ligands successfully. A similar kind of observation has been made for Mn coordinated [Mn-tetrafluoroterephthalate (4,4′-bipyridine) $(H_2O)_2$] MOF.[14] TGA (Figure 2c) shows that the synthesized MOF is thermally stable up to ∼340 °C, above which decomposition of the tricarboxylate linkers takes place with subsequent breakdown of the framework. After complete decomposition of carboxylate linkers at ∼480 °C, the residual material is converted into mixed valence Mn_3O_4. Elemental analysis shows that the carbon and hydrogen contents in the synthesized Mn-BTC MOF are 36.30% and 1.01%, respectively. From TGA, the wt % of Mn was calculated to be 23.6. This is in good agreement with ICP-AES analysis, which showed the presence of 24.5% of Mn in the MOF. Thus, combination of elemental analysis, TGA, and ICP-AES data corresponds to a composition of $Mn_3(BTC)_2$, for which the theoretical values of Mn, C, and H content are 24.01, 37.30, and 1.04%, respectively.[21] Accordingly, a schematic representation of the probable structural unit of Mn-BTC is given in Figure S1 in the Supporting Information. Figure 2, panel d shows Mn 2p high-resolution XPS spectrum for the as-synthesized Mn-BTC MOF. The spectrum consists of the spin−orbit split Mn $2p_{1/2}$ and $2p_{3/2}$ symmetric peaks appearing at ∼652.9 eV and ∼641 eV binding energies, respectively, along with pronounced satellite features appearing at 646.5 eV, that is, ∼5.5 eV to the higher binding energy side. These spectral features correspond to Mn predominantly in the Mn^{2+} state.[22] However, manganese having overlapping binding energy ranges for three oxidation states (II, III, IV) with significant multiplet splitting and another oxidation state (VI) with less defined splitting or broadening makes it difficult for quantitative analysis.[23] Morphology and microstructure of the synthesized Mn-BTC MOF were investigated through FESEM and TEM (Figure 3). FESEM images show a bar shaped morphology where the individual bars are about 1 μm wide and of varied lengths between 2 and 20 μm. TEM images reveal that these bars are made of porous sheets containing mesoporous walls and macroporous channels. Corrugated nature of the walls, as observed in Figure 3, panel d, may result from the unsaturated coordination of Mn. Such hierarchical porous structure would lead to improved electrolyte accessibility and thereby improved LIB performance by forming ion-buffering reservoir in the macropores, which would minimize the diffusion distances to the interior surfaces. On the other hand, the mesoporous walls would increase the active surface area and provide low resistance pathways for the ions.[24,25] The BET adsorption isotherm (Figure 4a) is convex in nature up to $P/P_0 = 1.0$, and a typical type-III isotherm with a discrete hysteresis loop starting from $P/P_0 \approx 0.5$ reveals a mixed H3 and H1 type indicating presence of interparticle as well as structural pores. The corresponding pore size distribution was calculated by Barrett−Joyner−Halenda (BJH) method using the desorption part (Figure 4b). A combination of mesopores with narrow size distribution (<4 to 12 nm) and macropores with broad size distribution (50−90 nm) has been observed indicating coexistence of structural pores as well as interparticle pores. BET surface area value is calculated to be 23.8 $m^2\ g^{-1}$ with corresponding pore volume of 0.0065 $cm^3\ g^{-1}\ nm^{-1}$. The observed surface area is somewhat lower than the values reported previously.[20] This is primarily due to the fact that the material was not subjected to any activation process following synthesis, which is commonly done for achieving a high surface area for MOFs. Also, rearrangement of pores during thermal removal of solvent may also contribute to the lowering of the surface area value. A very high surface area often leads to increased side reactions with the electrolyte particularly at lower potentials versus Li/Li^+ and thus may not be beneficial for LIB performance.

3.2. Electrochemical Characterization. The electrochemical performance of the as prepared Mn-BTC MOF versus Li/Li^+ was evaluated by cyclic voltammetry (CV) in the potential window 0.01−2.0 V to identify the redox processes, and the first four successive CV scans are presented in Figure 5, panel a. During the first cathodic scan, two broad peaks are observed at 0.47 and 0.32 V. These peaks are slightly shifted toward the left (0.41 and 0.26 V, respectively) after the initial scan, once the solid electrolyte interface (SEI) layer is formed. During the first anodic scan, a broad peak centered at around 0.99 V was observed, which deconvoluted into two broad peaks at ∼1.09 and ∼1.49 V during subsequent scans. These potential values being comparable to expected potential range for Mn^{3+} or Mn^{2+} to Mn^o reduction and the corresponding oxidation, occurrence of a conversion type reaction is indicated. However, FTIR spectroscopy and XRD analyses of the electrode material at the fully discharged (0.01 V) and charged (2.0 V) states failed to indicate presence of Mn^o in the discharged condition or MnO_2/Mn_3O_4 in the charged condition (Figure 1). Therefore, to ascertain whether the Li storage mechanism really involves conversion reaction or not, ex situ XPS

DOI: 10.1021/acsami.5b03414
ACS Appl. Mater. Interfaces 2015, 7, 16357−16363

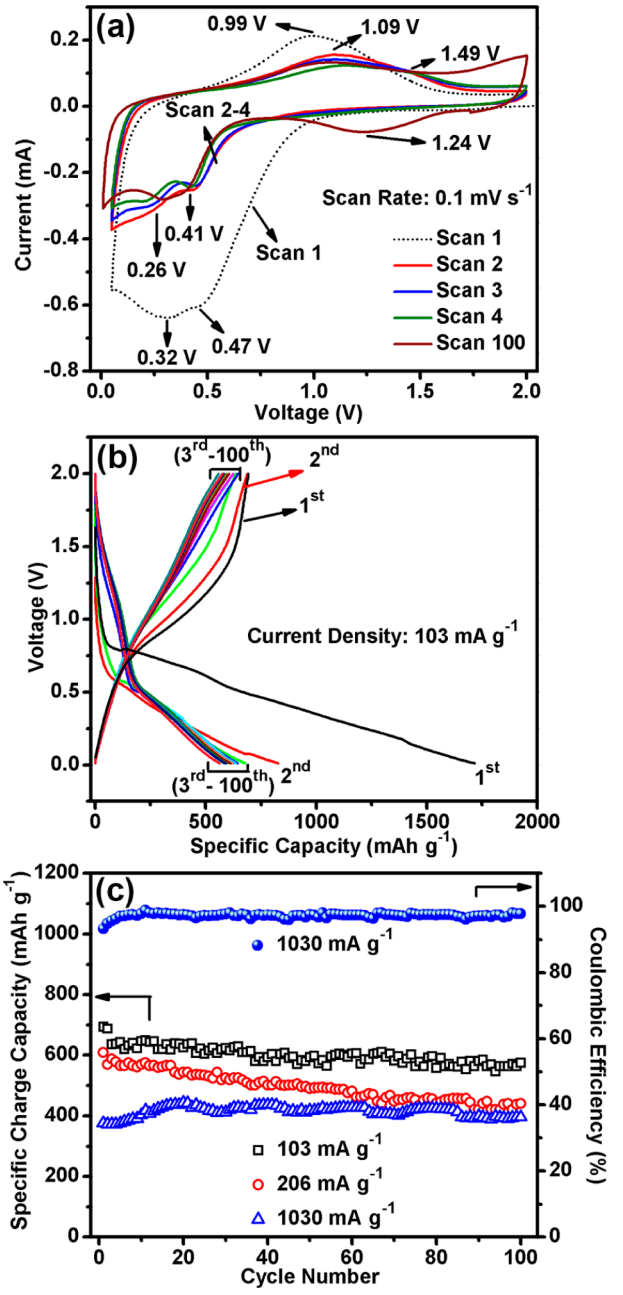

Figure 5. Electrochemical performance of Mn-BTC MOF: (a) cyclic voltammograms of Mn-BTC MOF at scanning rate of 0.1 mV s^{-1}; (b) galvanostatic discharge−charge profiles; (c) cycling performance.

Scheme 1. Probable Lithiation/Delithiation Sites for Coordination with Li in the Organic Moiety of Mn-BTC MOF

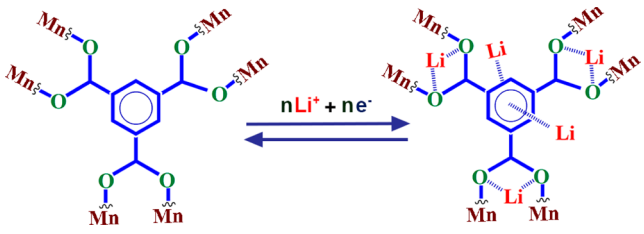

measurements of the electrode were carried out at the fully discharged state. Identical XPS spectra were observed (within

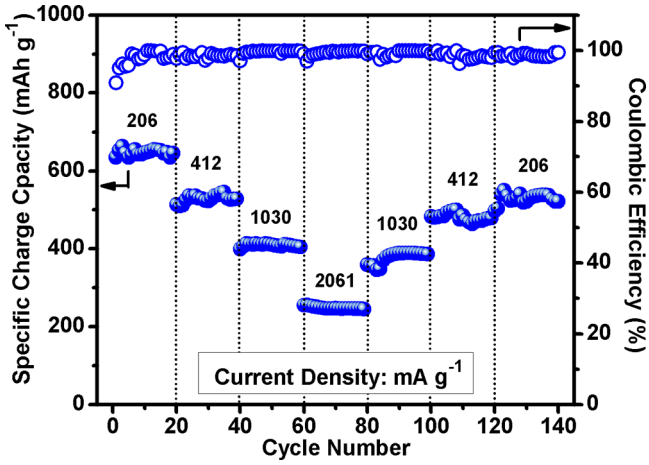

Figure 6. Rate performance of Mn-BTC MOF at different current densities from 0.2−2.0 A g^{-1}.

the experimental resolution) for both the cases: in the as-synthesized form and after full discharge to 0.01 V (Figure 2d). The spectral features consisting of higher binding energy satellites as well as the binding energy positions of the peaks clearly confirm the presence of manganese in the Mn^{2+} state and not in the Mn^{o} state after full discharge. Presence of Mn^{o} would have been reflected by appearance of an asymmetric peak and absence of any satellite peak. Thus, it appears that the usual conversion mechanism might not be applicable to explain the Li storage in Mn-BTC MOF. Armand et al.[16] have shown that lithium containing conjugated carboxylates, $Li_2C_6H_4O_4$ and $Li_2C_8H_4O_4$, being weakly electron withdrawing ligands, can act as redox centers for coordination of Li with COO^-. Therefore, it is likely that redox participation of the organic moiety through the COO^- groups plays an important role for Li insertion extraction in Mn-BTC MOF (Scheme 1). Thus, the observed reduction peaks could probably be attributed to insertion of Li^+ ion to the organic moiety without direct participation of manganese. Moreover, the very broad nature of the redox peaks is probably indicative of gradual multistep Li insertion process. Increasing repulsion between charges (e^-) due to gradual injection of Li^+ into the conjugated organic moieties would give rise to such behavior.[23] Therefore, the observed anodic peaks could tentatively be assigned to reversible Li deinsertion from the aromatic C_6 ring and the carboxylate moieties, respectively. However, further work is necessary to understand the exact mechanism. On the basis of the building unit shown in Figure S1, Supporting Information, there are a total number of 18 possible Li^+ insertion sites assuming that two oxygen atoms in the carboxylate moieties can attach one Li^+, and each aromatic ring can accommodate maximum of six numbers of Li^+. Thus, the calculated theoretical capacity would be 833 mAh g^{-1} (each Li insertion corresponds to ~46.3 mAh g^{-1}). The open circuit potential (OCP) of the as-assembled cells was 2.53 V. All the cells were subjected to an initial formation cycle at a low current density of 103 mA g^{-1} for effective formation of the SEI layer, and initial discharge and charge capacities of 1717 and 694 mAh g^{-1} were obtained with the first cycle Coulombic efficiency of 40% (Figure 5b). The OCP after the formation cycle was 1.29 V. The observed irreversible capacity loss can be attributed to increased side reactions with the electrolyte and formation of SEI layer. Selected individual discharge−charge profiles for the next 99 cycles are presented in Figure 5, panel b, where the reversibility

DOI: 10.1021/acsami.5b03414
ACS Appl. Mater. Interfaces 2015, 7, 16357−16363

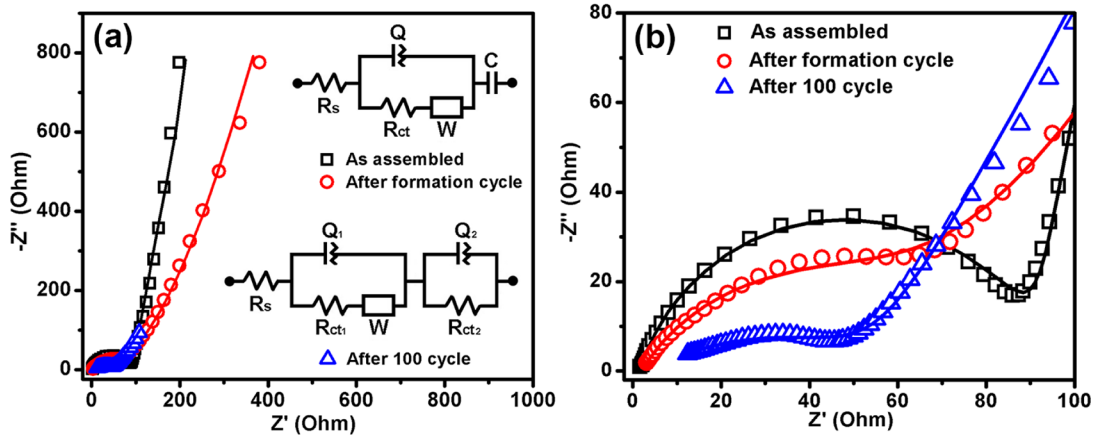

Figure 7. Impedance spectroscopic study of Mn-BTC MOF electrode at different cycling intervals: (a) low magnification image with equivalent circuits; (b) magnified view of the semicircles in the high frequency region.

Table 1. Fitted Data for Impedance Spectra at Different Cycling Stages

					Q_1 (constant phase element)		Q_2 (constant phase element)			
state of charge (V)	R_s (ohm)	R_{ct} (ohm)	R_{ct1} (ohm)	R_{ct2} (ohm)	Y_0' (μMho)	N'	Y_0'' (μMho)	N''	W (mMho)	C (mF)
as-assembled state (OCP)	1.59	84.3			17.9	0.82			7.89	1.30
after formation cycle (2 V)	1.97	67.3			67.4	0.66			1.92	1.47
after 100 cycle (2 V)	7.81		44.4	5.2	141	0.44	29.9	0.7	5.8	

of the two-step redox reactions is indicated. After the initial formation cycle, cycling performance Mn-BTC MOF has been tested in the potential window of 0.01−2.0 V at three different current densities of 103, 206, and 1030 mA g^{-1} for 100 continuous cycles at each rate, and the results are shown in Figure 5, panel c. A high specific capacity value of 694 mAh g^{-1} has been obtained at 103 mA g^{-1} with ∼83% retention after the 100th cycle. This is the highest reported capacity value for MOF anodes until now (Table S1, Supporting Information). At a high current density of ∼1.0 A g^{-1}, a steady specific capacity of ∼400 mAh g^{-1} could be achieved after a few initial cycles, with nearly 100% retention of capacity until the 100th cycle demonstrating an excellent cyclability (Figure 5c) and rate performance (Figure 6). Even at a very high current density of 2.06 A g^{-1}, a specific capacity of ∼250 mAh g^{-1} could be obtained. The gradual increase in the first 20 cycles may be due to equilibration and activation of the electrode at this very high current rate. After the few initial cycles, the Coulombic efficiency approaches 97% indicating excellent reversibility of the redox processes. This is also reflected by observation of nearly identical cyclic voltammograms after 100 cycles (Figure 5a). The conjugated carboxylates contain aromatic cores having a strong $\pi-\pi$ interaction that might have a significant role in stabilizing the MOF structure. To get further insight, electrochemical impedance spectroscopy has been carried out in the frequency range 10 mHz to 1 MHz with an AC amplitude of 10 mV for Mn-BTC MOF electrode at various cycling interval. The Nyquist plots in the as-assembled state, after the initial formation cycle and after 100 cycles, are presented in Figure 7, panel a and with an enlarged view of the high frequency region in Figure 7, panel b. The equivalent circuit models used to fit the impedance data are also shown in Figure 7, panel a, and the fitted parameters are summarized in Table 1. It is observed that the solution resistance (R_s) increases only slightly from 1.6 Ω in the as-assembled state to 7.8 Ω after 100 cycles, indicating a high degree of stability of the MOF with marginal electrochemical degradation. Also, the charge transfer resistance (R_{ct}) of the as-assembled sample decreases from 84.3 Ω to 67.3 Ω after the initial cycle and further to 44.4 Ω after 100 cycles, indicating better wetting of the electrodes and improved connectivity. A prominent capacitive nature is observed for the as-assembled cell, reflected by appearance of a near 90° spike in the low frequency region, which gradually diminishes with cycling and is nearly absent after 100 cycles.

4. CONCLUSIONS

In conclusion, by suitable choice of organic ligand, very high Li storage capacity in MOF is demonstrated where the redox reactions might not involve conversion mechanism; rather, the organic moiety appears to play an important role. Sustenance of the MOF network during cycling, high specific capacity of 694 mAh g^{-1} at 0.1 A g^{-1}, and a high rate performance together with a convenient potential of <2.0 V make Mn-BTC MOF a very promising anode for LIB applications. Further improvement in performance might be possible by grafting CNT into the Mn-BTC MOF network.

■ ASSOCIATED CONTENT

Supporting Information

Comparative performance of different MOFs as lithium-ion battery anode. A probable building unit of Mn-BTC MOF. The Supporting Information is available free of charge on the ACS Publications website at DOI: 10.1021/acsami.5b03414.

■ AUTHOR INFORMATION

Corresponding Author

*E-mail: mahanty@cgcri.res.in. Phone: +91-33-2322 3495. Fax: +91-33-2473 0957.

DOI: 10.1021/acsami.5b03414
ACS Appl. Mater. Interfaces 2015, 7, 16357−16363

Present Address

[§]CSIR-Institute of Minerals and Materials Technology, Bhubaneswar 751 013, India.

Notes

The authors declare no competing financial interest.

■ ACKNOWLEDGMENTS

The authors thank Director, CSIR-CGCRI for kind permission to publish this work. Financial support from CSIR via TAPSUN NWP0056 project is gratefully acknowledged.

■ REFERENCES

(1) Armand, M.; Tarascon, J. M. Building Better Batteries. *Nature* **2008**, *451*, 652−657.

(2) Kang, K.; Meng, Y. S.; Breger, J.; Grey, C. P.; Ceder, G. Electrodes with High Power and High Capacity for Rechargeable Lithium Batteries. *Science* **2006**, *311*, 977−980.

(3) Liu, C.; Li, F.; Ma, L. P.; Cheng, H. M. Advanced Materials for Energy Storage. *Adv. Mater.* **2010**, *22*, E28−E62.

(4) Hong, D.-Y.; Hwang, Y. K.; Serre, C.; Férey, G.; Chang, J.-S. Porous Chromium Terephthalate MIL-101 with Coordinatively Unsaturated Sites: Surface Functionalization, Encapsulation, Sorption and Catalysis. *Adv. Funct. Mater.* **2009**, *19*, 1537−1552.

(5) Liu, B. Metal-Organic Framework-Based Devices: Separation and Sensors. *J. Mater. Chem.* **2012**, *22*, 10094−10101.

(6) Nouar, F.; Eckert, J.; Eubank, J. F.; Forster, P.; Eddaoudi, M. Zeolite-like Metal-Organic Frameworks (ZMOFs) as Hydrogen Storage Platform: Lithium and Magnesium Ion-Exchange and H_2-(rho-ZMOF) Interaction Studies. *J. Am. Chem. Soc.* **2009**, *131*, 2864−2870.

(7) Kreno, L. E.; Leong, K.; Farha, O. K.; Allendorf, M.; Van Duyne, R. P.; Hupp, J. T. Metal-Organic Framework Materials as Chemical Sensors. *Chem. Rev.* **2012**, *112*, 1105−1125.

(8) Horcajada, P.; Chalati, T.; Serre, C.; Gillet, B.; Sebrie, C.; Baati, T.; Eubank, J. F.; Heurtaux, D.; Clayette, P.; Kreuz, C.; Chang, J.-S.; Hwang, Y. K.; Marsaud, V.; Bories, P.-N.; Cynober, L.; Gil, S.; Ferey, G.; Couvreur, P.; Gref, R. Porous Metal−organic-Framework Nanoscale Carriers as a Potential Platform for Drug Delivery and Imaging. *Nat. Mater.* **2010**, *9*, 172−178.

(9) Li, X.; Cheng, F.; Zhang, S.; Chen, J. Shape-Controlled Synthesis and Lithium-Storage Study of Metal-Organic Frameworks Zn_4O(1,3,5-benzenetribenzoate)$_2$. *J. Power Sources* **2006**, *160*, 542−547.

(10) Ferey, G.; Millange, F.; Morcrette, M.; Serre, C.; Doublet, M.-L.; Greneche, J.-M.; Tarascon, J.-M. Mixed-Valence Li/Fe-Based Metal−Organic Frameworks with Both Reversible Redox and Sorption Properties. *Angew. Chem., Int. Ed.* **2007**, *46*, 3259−3263.

(11) de Combarieu, G.; Morcrette, M.; Millange, F.; Guillou, N.; Cabana, J.; Grey, C. P.; Margiolaki, I.; Ferey, G.; Tarascon, J.-M. Influence of the Benzoquinone Sorption on the Structure and Electrochemical Performance of the MIL-53(Fe) Hybrid Porous Material in a Lithium-Ion Battery. *Chem. Mater.* **2009**, *21*, 1602−1611.

(12) Saravanan, K.; Nagarathinam, M.; Balaya, P.; Vittal, J. J. Lithium Storage in a Metal Organic Framework with Diamondoid Topology−A Case Study on Metal Formates. *J. Mater. Chem.* **2010**, *20*, 8329−8335.

(13) Han, X.; Yi, F.; Sun, T.; Sun, J. Synthesis and Electrochemical Performance of Li and Ni 1,4,5,8-Naphthalenetetracarboxylates as Anodes for Li-Ion Batteries. *Electrochem. Commun.* **2012**, *25*, 136−139.

(14) Liu, Q.; Yu, L.; Wang, Y.; Ji, Y.; Horvat, J.; Cheng, M.-L.; Jia, X.; Wang, G. Manganese-Based Layered Coordination Polymer: Synthesis, Structural Characterization, Magnetic Property, and Electrochemical Performance in Lithium-Ion Batteries. *Inorg. Chem.* **2013**, *52*, 2817−2822.

(15) Lin, Y.; Zhang, Q.; Zhao, C.; Li, H.; Kong, C.; Shen, C.; Chen, L. An Exceptionally Stable Functionalized Metal-Organic Framework for Lithium Storage. *Chem. Commun.* **2015**, *51*, 697−699.

(16) Armand, M.; Grugeon, S.; Vezin, H.; Laruelle, S.; Ribiere, P.; Poizot, P.; Tarascon, J.-M. Conjugated dicarboxylate anodes for Li-ion batteries. *Nat. Mater.* **2009**, *8*, 120−125.

(17) Ameloot, R.; Aubrey, M.; Wiers, B. M.; Gomora-Figueroa, A. P.; Patel, S. N.; Balsara, N. P.; Long, J. R. Ionic Conductivity in the Metal-Organic Framework UiO-66 by Dehydration and Insertion of Lithium *tert*-Butoxide. *Chem. - Eur. J.* **2013**, *19*, 5533−5536.

(18) Furukawa, H.; Cordova, K. E.; O'Keeffe, M.; Yaghi, O. M. The Chemistry and Applications of Metal-Organic Frameworks. *Science* **2013**, *341*, 1230444.

(19) Cheng, P.-C.; Lin, W.-C.; Tseng, F.-S.; Kao, C.-C.; Chang, T.-G.; Senthil Raja, D.; Liu, W.-R.; Lin, C.-H. Syntheses, Structures, and Properties of Multidimensional Lithium Coordination Polymers Based on Aliphatic Carboxylic Acids. *Dalton Trans.* **2013**, *42*, 2765−2772.

(20) Reinsch, H.; Stock, N. Formation and Characterisation of Mn-MIL-100. *CrystEngComm* **2013**, *15*, 544−550.

(21) Taylor, K. M. L.; Rieter, W. J.; Lin, W. Manganese-Based Nanoscale Metal-Organic Frameworks for Magnetic Resonance Imaging. *J. Am. Chem. Soc.* **2008**, *130*, 14358−14359.

(22) Guo, D.; Wu, Z.; An, Y.; Li, X.; Guo, X.; Chu, X.; Sun, C.; Lei, M.; Li, L.; Cao, L.; Li, P.; Tang, W. Room Temperature Ferromagnetism in $(Ga_{1-x}Mn_x)_2O_3$ Epitaxial Thin Films. *J. Mater. Chem. C* **2015**, *3*, 1830−1834.

(23) Biesinger, M. C.; Payne, B. P.; Grosvenor, A. P.; Lau, L. W. M.; Gerson, A. R.; Smart, R. St. C. Resolving Surface Chemical States in XPS Analysis of First Row Transition Metals, Oxides, and Hydroxides: Cr, Mn, Fe, Co, and Ni. *Appl. Surf. Sci.* **2011**, *257*, 2717−2730.

(24) Wang, D.-W.; Li, F.; Liu, M.; Lu, G. Q.; Cheng, H.-M. 3D Aperiodic Hierarchical Porous Graphitic Carbon Material for High-Rate Electrochemical Capacitive Energy Storage. *Angew. Chem., Int. Ed.* **2008**, *47*, 373−376.

(25) Giri, A. K.; Pal, P.; Ananthakumar, R.; Jayachandran, M.; Mahanty, S.; Panda, A. B. 3D Hierarchically Assembled Porous Wrinkled-Paper-like Structure of $ZnCo_2O_4$ and Co-ZnO@C as Anode Materials for Lithium-Ion Batteries. *Cryst. Growth Des.* **2014**, *14*, 3352−3359.

DOI: 10.1021/acsami.5b03414
ACS Appl. Mater. Interfaces 2015, 7, 16357−16363